

Reproducible evaluation of diffusion MRI features for automatic classification of patients with Alzheimer's disease

Junhao Wen^{a,b,c,d,e}, Jorge Samper-González,^{e,a,b,c,d} Simona Bottani^{e,a,b,c,d}, Alexandre Routier^{e,a,b,c,d,f}, Ninon Burgos^{a,b,c,d,e}, Thomas Jacquemont^{a,b,c,d,e}, Sabrina Fontanella^{a,b,c,d,e}, Stanley Durrleman^{e,a,b,c,d}, Stéphane Epelbaum^{a,b,c,d,e,g}, Anne Bertrand^{a,b,c,d,e,h*}, Olivier Colliot^{a,b,c,d,e,i}, for the Alzheimer's Disease Neuroimaging Initiative¹

^aInstitut du Cerveau et de la Moelle épinière, ICM, F-75013, Paris, France

^bInserm, U 1127, F-75013, Paris, France

^cCNRS, UMR 7225, F-75013, Paris, France

^dSorbonne Université, F-75013, Paris, France

^eInria, Aramis project-team, F-75013, Paris, France

^fInstitut du Cerveau et de la Moelle épinière, ICM, FrontLab, F-75013, Paris, France

^gAP-HP, Hôpital de la Pitié Salpêtrière, Institute of Memory and Alzheimer's Disease (IM2A), Centre of excellence of neurodegenerative disease (CoEN), Department of Neurology, F-75013, Paris, France.

^hAP-HP, Hôpital Saint-Antoine, Department of Radiology, F-75013, Paris, France

ⁱAP-HP, Hôpital de la Pitié Salpêtrière, Departments of Neurology and Neuroradiology, F-75013, Paris, France

* Deceased, March 2nd, 2018

¹ Data used in preparation of this article were obtained from the Alzheimer's Disease Neuroimaging Initiative (ADNI) database (adni.loni.usc.edu). As such, the investigators within the ADNI contributed to the design and implementation of ADNI and/or provided data but did not participate in analysis or writing of this report. A complete listing of ADNI investigators can be found at: http://adni.loni.usc.edu/wp-content/uploads/how_to_apply/ADNI_Acknowledgement_List.pdf

Correspondence to:

Olivier Colliot, PhD - olivier.colliot@upmc.fr

Junhao Wen - junhao.wen89@gmail.com

ICM – Brain and Spinal Cord Institute

ARAMIS team

Pitié-Salpêtrière Hospital

47-83, boulevard de l'Hôpital, 75651 Paris Cedex 13, France

ORCID number:

Olivier Colliot: 0000-0002-9836-654X

Junhao Wen: 0000-0003-2077-3070

Abstract

Diffusion MRI is the modality of choice to study alterations of white matter. In the past years, various works have used diffusion MRI for automatic classification of Alzheimer's disease. However, the performances obtained with different approaches are difficult to compare because of variations in components such as input data, participant selection, image preprocessing, feature extraction, feature selection (FS) and cross-validation (CV) procedure. Moreover, these studies are also difficult to reproduce because these different components are not readily available. In a previous work (Samper-González et al. 2018), we proposed an open-source framework for the reproducible evaluation of AD classification from T1-weighted (T1w) MRI and PET data. In the present paper, we extend this framework to diffusion MRI data. The framework comprises: tools to automatically convert ADNI data into the BIDS standard, pipelines for image preprocessing and feature extraction, baseline classifiers and a rigorous CV procedure. We demonstrate the use of the framework through assessing the influence of diffusion tensor imaging (DTI) metrics (fractional anisotropy - FA, mean diffusivity - MD), feature types, imaging modalities (diffusion MRI or T1w MRI), data imbalance and FS bias. First, voxel-wise features generally gave better performances than regional features. Secondly, FA and MD provided comparable results for voxel-wise features. Thirdly, T1w MRI performed better than diffusion MRI. Fourthly, we demonstrated that using non-nested validation of FS leads to unreliable and over-optimistic results. All the code is publicly available: general-purpose tools have been integrated into the Clinica software (www.clinica.run) and the paper-specific code is available at: <https://gitlab.icm-institute.org/aramislab/AD-ML>.

Keywords: classification, machine learning, reproducibility, Alzheimer's disease, diffusion magnetic resonance imaging, DTI, open-source

1. Introduction

Alzheimer's disease (AD), the most prevalent form of dementia, is expected to affect 1 out of 85 people in the world by the year 2050 (Brookmeyer et al. 2007). Neuroimaging offers the possibility to study pathological brain changes associated with AD in vivo (Ewers et al. 2011). The most common neuroimaging modalities used to study AD are T1-weighted (T1w) magnetic resonance imaging (MRI) and positron emission tomography (PET) with various tracers (Frisoni et al. 2010; Vemuri & Jack 2010). These techniques allow studying different types of alterations in the gray matter (GM). However, while AD is often considered primarily a gray matter disease, white matter (WM) is also extensively altered. There has thus been an increased interest in using diffusion MRI to study alterations in WM as the disease progresses (Fellgiebel et al. 2006; Kantarci et al. 2001; Müller et al. 2005; Müller et al. 2007).

In the past decades, there has been a strong interest in developing machine learning methods to assist diagnosis and prognosis of AD based on neuroimaging data (Rathore et al. 2017a; Falahati et al. 2014; Haller et al. 2011). In particular, a large number of studies using machine learning have looked at the potential of diffusion MRI for AD classification (Maggipinto et al. 2017; Dyrba, Barkhof, et al. 2015; Lella et al. 2017; Cui et al. 2012; Xie et al. 2015; Li et al. 2014). Several of these studies make use of the same publicly available dataset: the Alzheimer's Disease Neuroimaging Initiative (ADNI) (adni.loni.usc.edu). However, classification performances are not directly comparable across these studies because of differences in participant selection, feature extraction and selection, and performance metrics. It is thus difficult to know which approach performs best and which components of the method have the greatest influence on classification performances. We recently proposed a framework for the reproducible evaluation of machine learning algorithms in AD and demonstrated its use on PET and T1w MRI data (Samper-González et al. 2018). The framework is composed of tools for management of public datasets and in particular their conversion into

the Brain Imaging Data Structure (BIDS) format (Gorgolewski et al., 2016), standardized preprocessing pipelines, feature extraction tools and classification algorithms as well as procedures for evaluation. This framework was devoted to T1w MRI and PET data.

In the present work, we extend this framework to diffusion MRI data. We first perform a systematic review of the previous works devoted to automatic classification of AD using diffusion MRI data. We then present the different components of the framework, namely tools to convert ADNI diffusion MRI data into BIDS, preprocessing pipelines, feature extraction and selection methods and evaluation framework. We finally apply the framework to study the influence of various components on the classification performance: feature type (voxel-wise or regional features), imaging modality (T1w or diffusion MRI), data imbalance and feature selection (FS) strategy.

All the code (both of the framework and of the experiments) is publicly available: the general-purpose tools have been incorporated into Clinica (Routier et al. 2018), an open-source software platform that we developed for brain image analysis, and the paper-specific code is available at: <https://gitlab.icm-institute.org/aramislab/AD-ML>.

2. State of the art

AD is associated with altered integrity of WM, in particular the loss of cellular barriers that constrain free water motion (Xie et al. 2006). The fact that DTI was designed to study WM microstructure has led to the hypothesis that DTI-based features can be used for AD classification (Selnes et al. 2013). In recent years, a large body of research has been published for classification of AD using diffusion MRI. Here, we provide a review of these works.

We performed an online search of publications concerning classification of AD using diffusion MRI. We included only publications in English language, only original research publications (excluding review papers) and only peer-reviewed papers (either in journals or in conference proceedings), thereby excluding abstracts and preprints. We first searched on PubMed with the following search criteria: i) keywords: “(((classification diffusion MRI alzheimer's disease[Title/Abstract]) OR classification DTI alzheimer's disease[Title/Abstract]) OR diagnosis DTI alzheimer's disease[Title/Abstract]) OR diagnosis diffusion MRI alzheimer's disease[Title/Abstract]”, ii) publication date: before the 31st October 2018, and iii) study species: humans. We identified 616 studies based on these criteria. Among these studies, 105 review papers were excluded. Based on the abstract, we then selected only papers devoted to AD classification and using at least diffusion MRI. This resulted in 18 studies. Secondly, another query was performed on Scopus with the following criteria: i) keywords: “(TITLE-ABS-KEY(classification OR diagnosis) AND TITLE-ABS-KEY((diffusion AND mri) OR dti) AND TITLE-ABS-KEY((alzheimer's OR alzheimer) AND disease))”, and ii) publication date before the search day (the 31st October 2018). This resulted in 425 studies. We then excluded 104 review papers. Moreover, limiting to only peer-reviewed journals or conference proceedings resulted in 298 studies. Based on the abstract, we selected only papers devoted to AD classification and using at least diffusion MRI, resulting in 27 studies. After merging the studies found by both PubMed and Scopus, we obtained 32 studies. To complete this search,

we also did a search on Google Scholar with keywords: “classification diffusion MRI alzheimer's disease” or “classification DTI alzheimer's disease” or “diagnosis DTI alzheimer's disease” or “diagnosis diffusion MRI alzheimer's disease”. Two additional studies were included, resulting in a total of 34 studies which are presented in the current state-of-the-art section.

These 34 studies can be categorized according to the following criteria. i) *Studied modality*. While the majority used only diffusion MRI, some used multimodal data (combining diffusion MRI with T1w MRI or functional MRI for instance). ii) *Type of features*. We subdivided between papers using DTI metric features, such as fractional anisotropy (FA) and mean diffusivity (MD), and those using more advanced features, such as tract-based or network-based features. iii) *Classifiers*. The most commonly used are support vector machines (SVM) but random forests (RF), logistic regression (LR), nearest neighbors (NN) or naive Bayes (NB) were also used in some studies. iv) *Dataset*. The most commonly used dataset is the ADNI although it does not constitute an overwhelming majority, unlike for T1w-MRI or PET studies. This is probably because diffusion MRI was not present in ADNI1. v) *Classification tasks*. Some studies focused on the discrimination between AD patients and CN (cognitively normal) subjects while other tackled classification of patients with MCI (mild cognitive impairment) or prediction of progression to AD among MCI patients. A summary of these characteristics for the different studies is presented in Tables 1 (for those using DTI metric features) and Table 2 (for connectivity or tractography features). Besides, if multimodal imaging or different type of features (i.e., DTI metric and more advanced features) were used in a study, we reported the accuracy of the best performance.

Table 1. Summary of the studies using DTI metric features for AD classification.

Abbreviations: dMRI: diffusion MRI; T1w: T1-weighted MRI; fMRI: functional MRI.

SVM: support vector machine; RVM: relevance vector machine; RF: random forest; NB: naive Bayes; LR: logistic regression; NN: nearest neighbor.

1: accuracy; 2: area under the curve.

EDSD: European DTI Study on Dementia; MAS: Sydney Memory and Aging; RRMC: Research and Resource Memory; HSA: Hospital de Santiago Apostol; PRODEM: Prospective Registry on Dementia study; ADNI: Alzheimer's Disease Neuroimaging Initiative; IDC: IIsan Dementia Cohort; MCXWH: Memory Clinical at Xuan Wu Hospital; TJH: Tong Ji Hospital; MICPNU: Memory Impairment Clinic of Pusan National University Hospital; UHG: University Hospital of Geneva; DZNE: German Center for Neurodegenerative Diseases Rostock database; Local: private database.

RD: radial diffusivity; AD: axial diffusivity; MO: mode of anisotropy.

a: non-amnesic Mild Cognitive Impairment; b: amnesic Mild Cognitive Impairment; c: MCI-A β 42-; d: MCI-A β 42+; e: sd-aMCI, single domain amnesic MCI; f: sd-fMCI, single domain frontal MCI; g: md-aMCI, multiple domains amnesic MCI; h: late MCI; i: early MCI; --, not applicable.

Study	Subject			Modality	Feature	Classifier	Database	Performance			
	AD	MCI	CN					CN/ AD	CN/ MCI	sMCI/ pMCI	AD/ MCI
Ahmed et al. 2017	45	58	52	dMRI, T1w	Hippocampal voxel MD	SVM	ADNI	0.90 ¹	0.79 ¹	--	0.77 ¹
Cui et al. 2012	--	79 ^b	204	dMRI, T1w	Regional FA	SVM	MAS	--	0.71 ¹	--	--
Dyrba et al. 2013	137	--	143	dMRI	Voxel FA, MD	SVM	EDSD	0.83 ¹	--	--	--
Dyrba, Barkhof, et al. 2015	--	35 ^c , 42 ^d	25	dMRI, T1w	Voxel FA, MD, MO	SVM	EDSD	--	0.77 ^{1,d}	0.68 ¹	--
Dyrba, Grothe, et al. 2015	28	--	25	dMRI, T1w, fMRI	Regional FA, MD, MO	SVM	DZNE	0.89 ²	--	--	--
Demirhan et al. 2015	43	--	70	dMRI	Voxel and regional FA	SVM	ADNI	0.88 ¹	0.78 ¹	--	0.86 ¹
Friese et al. 2010	21	--	20	dMRI, T1w	Voxel FA, MD	LR	Local	0.88 ²	--	--	--
Graña et al. 2011	20	--	25	dMRI	Voxel FA, MD	SVM	HSA	1 ¹	--	--	--
Gao et al. 2015	--	41	63	dMRI, T1w, fMRI	Regional FA	--	UHG	--	0.85 ¹	--	--
Jung et al. 2015	27	18	--	dMRI, T1w	Regional FA, MD	SVM	MICPNU	--	--	--	0.87 ¹
Lee, Park, and Han 2015	35	73	33	dMRI	Voxel FA, MO	SVM	ADNI	0.88 ¹	--	--	0.90 ¹

Lella et al. 2017	40	--	40	dMRI	Voxel FA, MD	SVM, RF, NB	ADNI	0.78 ¹	--	--	--
Mesrob et al. 2012	15	--	16	dMRI, T1w	Voxel and regional FA, MD	SVM	RRMC	1 ¹	--	--	--
M. Li et al. 2014	21	--	15	dMRI, T1w	Regional FA	SVM	TJH	0.94 ¹	--	--	--
Maggipinto et al. 2017	90	90	89	dMRI	Voxel FA, MD	RF	ADNI	0.76 ¹	0.60 ¹	--	--
O'Dwyer et al. 2012	--	19 ^a , 14 ^b	40	dMRI	Voxel FA, MD, RD, AD	SVM	EDSD	--	0.93 ¹	--	--
S. Haller et al. 2013	--	18 ^e , 13 ^f , 35 ^g	--	dMRI	Voxel FA	SVM	Local	--	--	0.99 ^{1,e,f}	--
Schouten et al. 2016	77	--	173	dMRI, T1w, fMRI	Regional FA, MD	LR	PRODEM	0.95 ²	--	--	--
Termenon et al. 2011	15	--	20	dMRI	Voxel FA, MD	SVM, RVM, NN	HSA	0.99 ¹	--	--	--
Y. Xie et al. 2015	--	64 ^b	64	dMRI, T1w	Voxel FA, MD	SVM	MCXWH	--	0.84 ¹	--	--
Zhang and Liu 2018	48	39 ^b , 75 ⁱ	51	dMRI	Regional FA, MD, RD, AD	SVM, LR	ADNI	0.90 ¹	--	0.93 ¹	--

Table 2. Summary of the studies using tract-based or network-based features for AD classification.

Abbreviations: dMRI: diffusion MRI; T1w: T1-weighted MRI; fMRI: functional MRI.

SVM: support vector machine; LDA: linear discriminant analysis; RF: random forest; NB: naive bayes; LR: logistic regression; NN: nearest neighbor.

1: balanced accuracy; 2: accuracy; 3: area under the curve.

DUBIAC: Duke-UNC Brain Imaging and Analysis Center; RRMCM: Research and Resource Memory; PRODEM: Prospective Registry on Dementia study; ADNI: Alzheimer's Disease Neuroimaging Initiative; NACC: National Alzheimer's Coordinating Center; NorCog: Norwegian registry for persons being evaluated for cognitive symptoms in specialized health care.

a: subjective decline MCI; b: late MCI; c: early MCI; --, not applicable.

Study	Subject			Modality	dMRI Feature	Classifier	Database	Performance			
	AD	MCI	CN					CN/ AD	CN/ MCI	sMCI/ pMCI	AD/ MCI
Amoroso et al. 2017	47	--	52	dMRI	Network measures	--	ADNI	0.95 ³	--	--	--
Cai et al. 2018	165	--	165	dMRI, T1w	Network measures	LDA	ADNI	0.85 ²	--	--	--
Doan et al. 2017	79	55, 30 ^a	--	dMRI	Tract measures, regional FA, MD, RD, AD	LR	NorCog	--	--	--	0.71 ³
Ebadi et al. 2017	15	15	15	dMRI	Network measures	LR, RF, NB, SVM, NN	--	0.80 ²	0.70 ²	--	0.80 ²
Lee, Park, and Han 2013	--	39	39	dMRI	Tract measures, voxel and regional FA	SVM	ADNI	--	1 ²	--	--
Lella et al. 2018	40	30	52	dMRI	Network measures	SVM	ADNI	0.77 ³	--	--	--
Nir et al. 2015	37	113	50	dMRI	Tract measures, FA, MD	SVM	ADNI	0.85 ²	0.79 ²	--	--
Prasad et al. 2015	38	38 ^b , 74 ^c	50	dMRI	Network measures	SVM	ADNI	0.78 ²	--	0.63 ²	--
Schouten et al. 2017	77	--	173	dMRI	Network measures, voxel FA, MD, RD, AD	LR	PRODEM	0.92 ²	--	--	--
Wee et al. 2012	--	10	17	dMRI, fMRI	Network measures	SVM	DUBIAC	--	0.96 ²	--	--
Wang et al. 2018	--	169	379	dMRI, T1w	Network measures	SVM, RF	ADNI, NACC	--	0.75 ³	--	--
Zhu et al. 2014	--	22	22	dMRI, fMRI	Network measures	SVM	NACC	--	0.95 ²	--	--
Zhan et al. 2015	39	112	51	dMRI	Network measures	LR	ADNI	0.71 ¹	0.57 ¹	--	0.69 ¹

Twenty-one studies used DTI metrics as features (see details in Table 1). Among the DTI derived metrics, FA and MD were most frequently used (O'Dwyer et al. 2012; Maggipinto et al. 2017; Dyrba et al. 2013; Dyrba, Barkhof, et al. 2015; Lella et al. 2017; Mesrob et al. 2012; Zhang & Liu 2018; Termenon et al. 2011; Xie et al. 2015; Frieze et al. 2010; Schouten et al. 2016; Jung et al. 2015; Dyrba, Grothe, et al. 2015). Besides, radial diffusivity (RD), axial diffusivity (AD) and mode of anisotropy (MO) were also examined in some papers (O'Dwyer et al. 2012; Dyrba, Barkhof, et al. 2015; Lee et al. 2015; Zhang & Liu 2018; Dyrba, Grothe, et al. 2015). Voxel- and region-wise features were both used. For voxel-wise classification, all voxels from the segmented GM or WM were used. For region-wise classification, the mean value within each region of interest (ROI) of DTI metric maps were extracted using an anatomical atlas. The most commonly used atlases were the John Hopkins University (JHU) atlases (Hua et al. 2008). Ten studies adopted only diffusion MRI for AD classification (O'Dwyer et al. 2012; Maggipinto et al. 2017; Dyrba et al. 2013; Lella et al. 2017; Zhang & Liu 2018; Termenon et al. 2011; Demirhan et al. 2015; Haller et al. 2013; Graña et al. 2011; Lee et al. 2015). The other eleven studies looked at the potential of multimodal MRI, for instance T1w MRI and diffusion MRI, for AD diagnosis and compared the performances cross modalities. For the DTI metric-based studies, SVM was most frequently used (O'Dwyer et al. 2012; Dyrba et al. 2013; Dyrba, Barkhof, et al. 2015; Lella et al. 2017; Cui et al. 2012; Mesrob et al. 2012; Zhang & Liu 2018; Termenon et al. 2011; Xie et al. 2015; Jung et al. 2015; Demirhan et al. 2015; Ahmed et al. 2017; Li et al. 2014; Lee et al. 2015; Graña et al. 2011; Haller et al. 2013; Dyrba, Grothe, et al. 2015).

Thirteen works demonstrated the usage of more complex features, such as tract-based or network-based features (see details in Table 2). In such approaches, tractography is used to extract WM tracts from diffusion MRI data. To be reliable, such a procedure requires to have high angular resolution diffusion imaging data. Then, tract-based approaches compute indices

that characterize the tract, including tract volume, average FA/MD across the tract or more advanced features (Doan et al. 2017; Nir et al. 2015; Lee et al. 2013). Such indices are used as input of the classifier. In network-based features, the result of the tractography (also called the tractogram) is used to build a graph of anatomical connections. Usually, the GM is parcellated into a set of anatomical regions and the connectivity between two given regions is computed based on the tractogram. To that purpose, different measures have been used, including the number of fibers or the average FA along the connection. This results in a connectivity network which can be described through network-based measures. Such features characterize the local and global topology of the network and are fed to a classifier. Ten studies used network-based features derived from diffusion MRI for AD classification (Schouten et al. 2017; Ebadi et al. 2017; Prasad et al. 2015; Wee et al. 2012; Cai et al. 2018; Lella et al. 2018; Wang et al. 2018; Zhan et al. 2015; Amoroso et al. 2017; Zhu et al. 2014).

There is a high variability in terms of classification performances across studies. For DTI metric features, the classification accuracy ranges from 0.71 to 1 for task CN vs AD. With regard to the accuracies across types of features, no consistency existed across studies. For instance, Nir et al observed that, in their study, the performances of MD outperformed FA (Nir et al. 2015). However, O'Dwyer et al reported higher accuracy for FA than MD in their experiments (O'Dwyer et al. 2012) and another study obtained comparable accuracies for both metrics (Dyrba et al. 2013). Conflicting results were also reported for the comparison of different modalities. Mesrob et al obtained higher accuracy with T1w MRI than with diffusion MRI (Mesrob et al. 2012) while Dyrba et al came to the opposite conclusion (Dyrba, Barkhof, et al. 2015). For network- or tract-based features, the classification accuracy ranges from 0.71 to 0.95 for task CN vs AD, a range which is comparable to that obtained with DTI metrics.

In this work, we choose to focus on DTI metrics because: i) they are more simple than connectivity or tractography features; ii) they can be easily computed and can make use of

standard diffusion MRI sequences, thus are more adapted to translation to clinical practice, iii) to date, there is no clear evidence that connectivity/tractography features lead to higher accuracies for AD classification and iv) conflicting results exist regarding the respective performance of different DTI metrics in this context.

3. Materials

The data used in the preparation of this article were obtained from the Alzheimer's Disease Neuroimaging Initiative database (ADNI) (adni.loni.usc.edu). The ADNI was launched in 2003 as a public-private partnership, led by Principal Investigator Michael W. Weiner, MD. The primary goal of ADNI has been to test whether serial MRI, PET, other biological markers, and clinical and neuropsychological assessment can be combined to measure the progression of MCI and early AD. Over 1,650 participants were recruited across North America during the first three phases of the study (ADNI1, ADNI GO and ADNI2). Around 400 participants were diagnosed with AD, 900 with MCI and 350 were control subjects. Three main criteria were used to classify the subjects (Petersen et al. 2010). The normal subjects had no memory complaints, while the subjects with MCI and AD both had to have complaints. CN and MCI subjects had a mini-mental state examination (MMSE) score between 24 and 30 (inclusive), and AD subjects between 20 and 26 (inclusive). The CN subjects had a clinical dementia rating (CDR) score of 0, the MCI subjects of 0.5 with a mandatory requirement of the memory box score being 0.5 or greater, and the AD subjects of 0.5 or 1. The other criteria can be found in (Petersen et al. 2010).

Five diagnosis groups were considered:

- CN: subjects who were diagnosed as CN at baseline;
- AD: subjects who were diagnosed as AD at baseline;
- MCI: subjects who were diagnosed as MCI, EMCI or LMCI at baseline;
- pMCI: subjects who were diagnosed as MCI, EMCI or LMCI at baseline, were

followed during at least 36 months and progressed to AD between their first visit and the visit at 36 months;

- sMCI: subjects who were diagnosed as MCI, EMCI or LMCI at baseline, were followed during at least 36 months and did not progress to AD between their first visit and the visit at 36 months.

Naturally, all participants in the pMCI and sMCI groups are also in the MCI group. Note that the reverse is false, as some MCI subjects did not convert to AD but were not followed long enough to state whether they were sMCI or pMCI.

The diffusion-weighted images (DWIs) of ADNI were downloaded in October 2016. They all came from ADNI GO and ADNI2 phases. Two different acquisition protocols are described for DWIs: Axial DTI (images with “Sequence” field starting by “AX_DTI” and “Axial_DTI” in the file of “IDA_MR_Metadata_Listing.csv”) and Enhanced Axial DTI (images with “Sequence” field equal to “Enhanced_Axial_DTI” in the file of “IDA_MR_Metadata_Listing.csv”). In total, Axial DTI were available for 1019 visits and Enhanced Axial DTI for 102 visits. Only Axial DTI images were available for the baseline visit (222). In the current study, we included the participants whose diffusion and T1w MRI scans were both available at baseline. These DWIs were acquired with the following parameters: 35 cm field of view, 128×128 acquired matrix, reconstructed to a 256×256 matrix; voxel size: 1.35×1.35×2.7mm ; scan time = 9 min; 41 diffusion-weighted directions at b-value = 1000 s/mm² and 5 T2-weighted images (b-value = 0 s/mm², referred to as b0 image). Besides, each participant underwent a T1w MRI sequence with following parameters: 256×256 matrix; voxel size = 1.2×1.0×1.0 mm ; TI = 400 ms; TR = 6.98 ms; TE = 2.85 ms; flip angle = 11°. We used quality check (QC) information provided by ADNI to select participants (see below Section 4.1). Moreover, QC was conducted on the results of the preprocessing pipeline (see below Section 4.2). Four participants were excluded because of the lower image resolution (4.5×4.5×4.5mm). Finally, 46 CN, 97 MCI, 54 sMCI, 24 pMCI and 46 AD were included.

Table 3 summarizes the demographics, and the MMSE and global CDR scores of the participants in this study.

Table 3. Summary of participant demographics, mini-mental state examination (MMSE) and global clinical dementia rating (CDR) scores. Values are presented as mean \pm SD [range]. M: male, F: female

	N	Age	Gender	MMSE	CDR
CN	46	72.7 \pm 6.0 [59.8, 89.0]	21 M / 25 F	28.9 \pm 1.4 [24,30]	0: 46
MCI	97	72.9 \pm 7.3 [55.0, 87.8]	62 M / 35 F	27.7 \pm 1.7 [24,30]	0.5: 97
sMCI	54	72.6 \pm 7.7 [55.0, 87.8]	21 M / 25 F	28.0 \pm 1.7 [24,30]	0.5: 54
pMCI	24	74.2 \pm 6.1 [56.5, 85.3]	16 M / 8 F	26.8 \pm 1.4 [24,30]	0.5: 24
AD	46	74.4 \pm 8.4 [55.6, 90.3]	28 M / 18 F	23.4 \pm 1.9 [20,26]	0.5: 17; 1: 29;

4. Methods

The classification framework is illustrated in Figure 1. It includes: tools for data management, image processing, feature extraction and selection, classification, and evaluation. Conversion tools allow an easy update of ADNI as new subjects become available. To facilitate future development and testing, the different components were designed in a modular-based architecture: processing pipelines using Nipype (Gorgolewski et al. 2011), and classification and evaluation tools using the scikit-learn² library (Pedregosa et al., 2011). Thus the objective measurement of the impact of each component on the results could be clarified. A simple command line interface is provided and the code can also be used as a Python library.

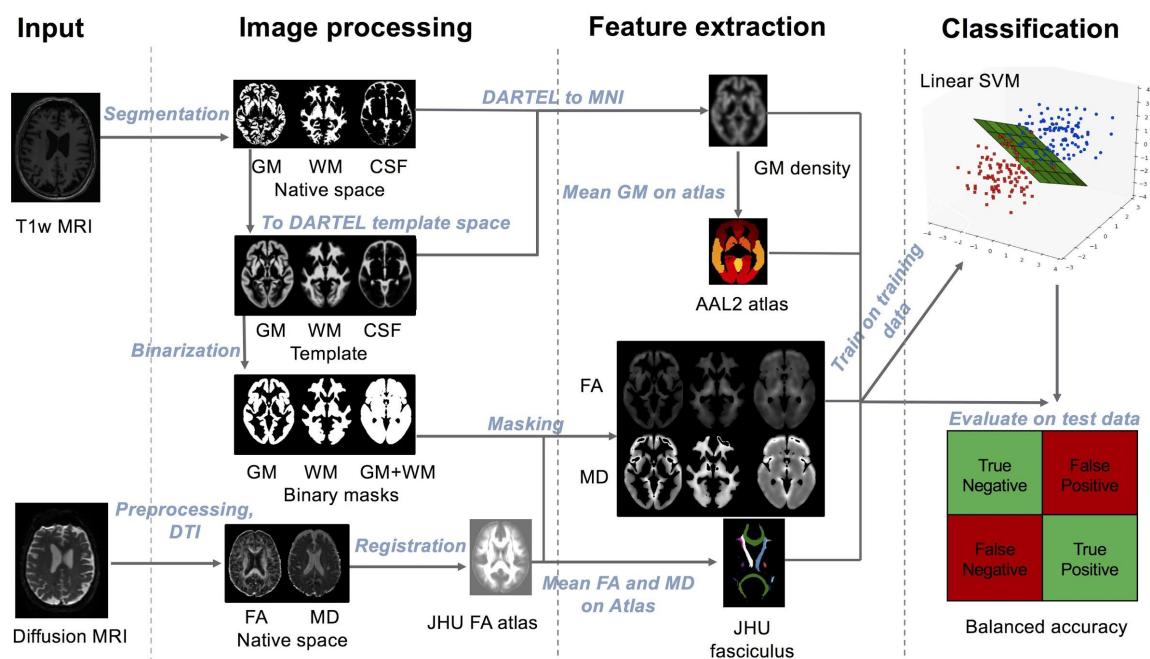


Figure 1. Overview of the framework.

² <http://scikit-learn.org>

4.1 Converting datasets to a standardized data structure

Public datasets, such as ADNI, are extremely useful to the research community. However, using the ADNI can be difficult because the downloaded raw data does not possess a clear and uniform organization. We thus proposed to convert ADNI data into the BIDS format (Gorgolewski et al. 2016), a community standard which allows storing multiple neuroimaging modalities as well as clinical and sociodemographic data. BIDS is based on a file hierarchy rather than on a database management system. It can thus be easily deployed in any research laboratory.

The ADNI to BIDS converter that we developed allows to automatically convert the raw dataset downloaded from the ADNI website to BIDS. The converter requires that the user has downloaded all the ADNI study data (tabular data in csv format) and the imaging data of interest. Importantly, the downloaded files must be kept exactly as they were downloaded. All conversion steps are then performed by the automatic converter, requiring no user intervention.

Details regarding conversion of clinical, sociodemographic and T1w MRI data can be found in (Samper-González et al. 2018). For the DWIs, first, we selected from the file “IDA_MR_Metadata_Listing.csv”, all entries containing “DTI” in the “Sequence” field. Images with a sequence name containing “Enhanced” were discarded. Then, “IMAGEUID” field was matched to corresponding “loni_image” field of ‘MAYOADIRL_MRI_IMAGEQC_12_08_15.csv’ file, to find QC information for each image. In cases where there existed several scans for a visit, we kept the one marked as selected (1 in ‘series_selected’ field of QC csv file). If there was no image marked as selected, then we chose the image with the best quality, (as specified in “series_quality” field, ranging from 1 to 4, 1 being excellent and 4 being unusable), excluding the images that failed QC (series_quality = 4). If there were several images for the same visit and QC information was not present, we chose the scan that was acquired the first. Once paths for each of the selected images were

gathered, the images in dicom format were converted to nifti format using the *dcm2niix*³ tool, or in case of error the *dcm2nii*⁴ tool (Li et al. 2016). Images failing the conversion using both tools were manually discarded. Finally, the converted images in nifti format were organised in the corresponding BIDS folder. Note that all these steps are automatically performed by the converter.

We also provide tools for subject selection according to the duration of follow up and the diagnose. In the present study, all the participants whose T1w MRI and diffusion MRI scans were available at baseline were included. Finally, we organized all the outputs of the experiments into a BIDS-inspired standardized structure.

4.2 Preprocessing pipelines

4.2.1 Preprocessing of T1w MRI

The image processing pipeline for T1w MRI was previously described in (Samper-González et al. 2018). In brief, the Unified Segmentation procedure (Ashburner & Friston 2005) is first used to simultaneously perform tissue segmentation, bias correction and spatial normalization of the input image. Next, a group template is created using DARTEL (Ashburner 2007), from the subjects' tissue probability maps in native space obtained at the previous step. Lastly, the DARTEL to MNI method (Ashburner 2007) is applied, providing a registration of the native space images into the MNI space. Besides, the GM and WM tissue maps from DARTEL template were binarized (with a threshold of 0.3) to obtain the corresponding tissue masks that are subsequently used in diffusion MRI pipeline.

³<https://github.com/rordenlab/dcm2niix>

⁴<https://www.nitrc.org/plugins/mwiki/index.php/dcm2nii:MainPage>

4.2.2 Preprocessing of diffusion MRI

For each subject, all b0 images were rigidly registered to the first b0 image and then averaged as the b0 reference. The raw DWIs were corrected for eddy current-induced distortions and subject movements by simultaneously modelling the effects of diffusion eddy currents and movements on the image using *eddy* tool (Andersson & Sotiropoulos 2016) from FMRIB Software Library (FSL) software (Jenkinson et al. 2012). To correct for susceptibility-induced distortions, as fieldmap data were not available in ADNI GO or ADNI2, the T1w MRI was used instead in this context. The skull-stripped b0 image was registered to the T1w MRI with two sequential steps: first a rigid registration using FSL *flirt* tool and then a non-linear registration using SyN registration algorithm from ANTs (Avants et al. 2008). SyN is an inverse-consistent registration algorithm allowing EPI induced susceptibility artifacts correction (Leow et al. 2007). Finally, the DWI volumes were corrected for nonuniform intensity using the ANTs N4 bias correction algorithm (Tustison & Avants 2013) and the diffusion weighting directions were appropriately updated (Leemans & Jones 2009). The implementation of these different steps is available in the *dwi-preprocessing-using-t1* pipeline of Clinica.

We performed QC on the results of the preprocessing pipeline. Specifically, we inspected the results for the presence of head motion artifacts and eddy current artifacts. Registration quality was also visually checked by overlapping the source image onto the target image. All preprocessed data were considered of acceptable quality.

The DTI model was then fitted to generate FA and MD maps using MRtrix (Tournier et al. 2012). FA maps were nonlinearly registered onto the JHU atlas FA template in MNI space with the ANTs SyN algorithm (Avants et al. 2008). The estimated nonlinear deformation was finally applied to the MD maps to have all the FA and MD maps in the same space. These procedures were implemented in the *dwi-processing-dti* pipeline of Clinica.

4.3 Feature extraction

We extracted two types of features: voxel-wise and regional features. After image preprocessing, all T1w MRI and diffusion MRI are in MNI space and we have a voxel-wise correspondence across subjects. Voxel-wise features simply correspond to all the voxels in GM for T1w MRI. In order to extract the DTI-based voxel-wise features, FA and MD maps were masked using the tissue masks (i.e., WM, GM and GM+WM tissue binarized masks) obtained from T1w MRI pipeline. Then a Gaussian smoothing kernel with full width at half maximum (fwhm) at 8 mm was applied to the masked FA and MD maps. The resulting maps were masked again by the tissue masks. Thus voxels in GM, WM or GM+WM tissue maps were used as voxel-wise features for diffusion MRI. Regional features correspond to the average value (GM density for T1w MRI; FA or MD for diffusion MRI) computed in a set of ROIs obtained from different atlases. AAL2 atlas containing 120 ROIs (Rolls et al. 2015) was used for T1w MRI. Two JHU atlases, ICBM-DTI-81 white-matter labels atlas (referred as JHULabel with 48 ROIs) and JHU white-matter tractography atlas with a 25% threshold (referred as JHUTract25 with 20 ROIs), were used for diffusion MRI. The different features are shown in Table 4.

Table 4. Summary of the different types of features.

Modality	Feature Type	Feature
Diffusion MRI	Voxel-wise	WM-FA
		WM-MD
		GM-FA
		GM-MD
		WM+GM-FA
		WM+GM-MD
	Region-wise	JHULabel-FA/MD
		JHUTract25-FA/MD
T1w MRI	Voxel-wise	GM-Density
	Region-wise	AAL2

4.4 Classification

Classification was performed using a linear SVM for both voxel-wise and regional features. As output of the classification, we reported the balanced accuracy, AUC, accuracy, sensitivity, specificity. Additionally, the optimal margin hyperplane (OMH) coefficient maps were reported. The OMH coefficient map represents the influence of each voxel or region on the classification performance. Thus, the OMH coefficient map characterizes the potential anatomical patterns associated to a given classifier (Cuingnet et al. 2013).

4.5 Cross-validation

As emphasized in the recent literature (Varoquaux et al. 2017), it is important to properly perform the cross-validation (CV) procedures. In the present work, the CV procedure included two nested loops: an outer loop evaluating the classification performances and an inner loop used to optimize the hyperparameters of the model (C for SVM). More precisely, repeated random splits (all of them stratified) with 250 repetitions was used for outer CV. For hyperparameter optimization, we used an inner loop with 10-fold CV. For each split, the model with the highest balanced accuracy is selected, and then these selected models are averaged across splits to profit of model averaging.

When FS is performed, it is crucial that FS is adequately incorporated into the CV procedure. FS is a process to identify relevant features and thereby reduce the dimensionality. It has the potential to reduce overfitting (Bermingham et al. 2015). In the present work, we aim to explore the impact of FS bias. The FS bias, also known as non-nested FS strategy, arises when FS is performed on the entire dataset and not within the CV procedure, thus introducing data leakage. On the contrary, a nested FS is a procedure blind to the test data and embedded into the nested CV (Maggipinto et al. 2017).

Two different FS algorithms were applied: an ANOVA univariate test and an embedding SVM recursive feature elimination (SVM-RFE) (Guyon et al. 2002; Chandrashekar & Sahin 2014). Specifically, the ANOVA test can be seen as a filter without taking the classifier into account and was performed for each feature independently. SVM-RFE uses the coefficients from the SVM models to assess feature importance. Then the least important features, which have the least effect on classification, are iteratively pruned from the current set of features. The remaining features are kept for the next iteration until the desired number of features has been obtained. For both methods, we tested varying numbers of selected features

(1% of the total number of features and then from 10% to 100%, increasing by 10% at each step).

4.6 Classification experiments

Four different classification tasks were considered: CN vs AD, CN vs pMCI, sMCI vs pMCI and CN vs MCI.

For all classification tasks, we assessed the influence of different components on the performance. First of all, we compared the performance obtained with different DTI metrics (FA, MD), different feature types (voxel, regional) and different atlases. Secondly, we compared the classification performance between diffusion MRI and T1w MRI. To note, the nested CV procedure, in each iteration, guaranteed the same subjects for data split (i.e., training and testing data) between modalities. Thirdly, we studied the impact of imbalanced data. Three tasks (i.e., CN vs pMCI, CN vs MCI and sMCI vs pMCI) have imbalanced data: the number of subjects of the majority group is nearly twice as many as that of the minority group. To assess the impact of data imbalance, a random down-sampling technique was used for each imbalanced task. In each iteration of the outer CV, this technique randomly excluded certain subjects from the majority group to ensure the subject balance between groups. Lastly, we evaluated the effect of FS bias.

5. Results

Here, we present the results of classification tasks using original data or balanced data in Tables 5 and 6. Balanced accuracy was used as performance metric. All the results with other performance metrics are available at <https://gitlab.icm-institute.org/aramislab/AD-ML>.

Table 5. Results of all the classification experiments using original (imbalanced) data. Balanced accuracy was used as performance metric. Values are presented as mean \pm standard deviation (SD).

Imaging Modality	Feature	CN vs AD	CN vs pMCI	sMCI vs pMCI	CN vs MCI
Diffusion MRI	WM-FA	0.73 \pm 0.099	0.52 \pm 0.108	0.43 \pm 0.088	0.57 \pm 0.090
	WM-MD	0.71 \pm 0.098	0.53 \pm 0.087	0.49 \pm 0.048	0.59 \pm 0.068
	GM-FA	0.71 \pm 0.097	0.59 \pm 0.107	0.48 \pm 0.089	0.57 \pm 0.088
	GM-MD	0.76 \pm 0.095	0.61 \pm 0.115	0.51 \pm 0.098	0.60 \pm 0.084
	WM+GM-FA	0.71 \pm 0.099	0.59 \pm 0.112	0.47 \pm 0.094	0.58 \pm 0.086
	WM+GM-MD	0.76 \pm 0.098	0.60 \pm 0.118	0.51 \pm 0.106	0.60 \pm 0.088
	JHULabel-FA	0.70 \pm 0.107	0.51 \pm 0.112	0.47 \pm 0.088	0.57 \pm 0.081
	JHULabel-MD	0.50 \pm 0	0.50 \pm 0	0.50 \pm 0	0.50 \pm 0
	JHUTract25-FA	0.66 \pm 0.102	0.54 \pm 0.118	0.47 \pm 0.078	0.55 \pm 0.077
	JHUTract25-MD	0.47 \pm 0	0.50 \pm 0	0.50 \pm 0	0.50 \pm 0
T1w MRI	GM-Density	0.88 \pm 0.066	0.73 \pm 0.112	0.64 \pm 0.113	0.58 \pm 0.086
	AAL2	0.86 \pm 0.073	0.69 \pm 0.120	0.64 \pm 0.118	0.59 \pm 0.090

Table 6. Results of all the classification experiments using balanced data. Balanced accuracy was used as performance metric. Values are presented as mean \pm standard deviation (SD).

Imaging Modality	Feature	CN vs pMCI	sMCI vs pMCI	CN vs MCI
Diffusion MRI	WM-FA	0.55 \pm 0.151	0.44 \pm 0.150	0.56 \pm 0.113
	WM-MD	0.61 \pm 0.140	0.48 \pm 0.138	0.55 \pm 0.090
	GM-FA	0.60 \pm 0.137	0.47 \pm 0.151	0.59 \pm 0.1073
	GM-MD	0.62 \pm 0.144	0.51 \pm 0.146	0.57 \pm 0.101
	WM+GM-FA	0.61 \pm 0.146	0.44 \pm 0.156	0.57 \pm 0.110
	WM+GM-MD	0.62 \pm 0.139	0.51 \pm 0.150	0.57 \pm 0.105
	JHULabel-FA	0.53 \pm 0.138	0.47 \pm 0.138	0.57 \pm 0.101
	JHULabel-MD	0.55 \pm 0.088	0.48 \pm 0.142	0.58 \pm 0.078
	JHUTract25-FA	0.57 \pm 0.135	0.48 \pm 0.142	0.54 \pm 0.118
	JHUTract25-MD	0.64 \pm 0.148	0.53 \pm 0.144	0.59 \pm 0.103

5.1 Influence of the type of features

Generally, voxel-wise features provided higher accuracies than regional features. While the difference was moderate for FA, it was particularly striking for MD: MD region-wise classifications did not perform better than chance for all tasks. In general, for voxel-wise features, the performances obtained with FA and MD were of the same order of magnitude. However, one can note that accuracies were (moderately but systematically) higher for MD

than for FA. Finally, for MD, the inclusion of GM (either in isolation or when combined with WM) considerably increased the performance over the use of WM alone (see Table 5).

5.2 Influence of the imaging modality

Compared to diffusion MRI, T1w MRI lead to higher accuracies for tasks CN vs AD, CN vs pMCI and sMCI vs pMCI (Figure 2). On the other hand, both modalities led to low performance for the task CN vs MCI.

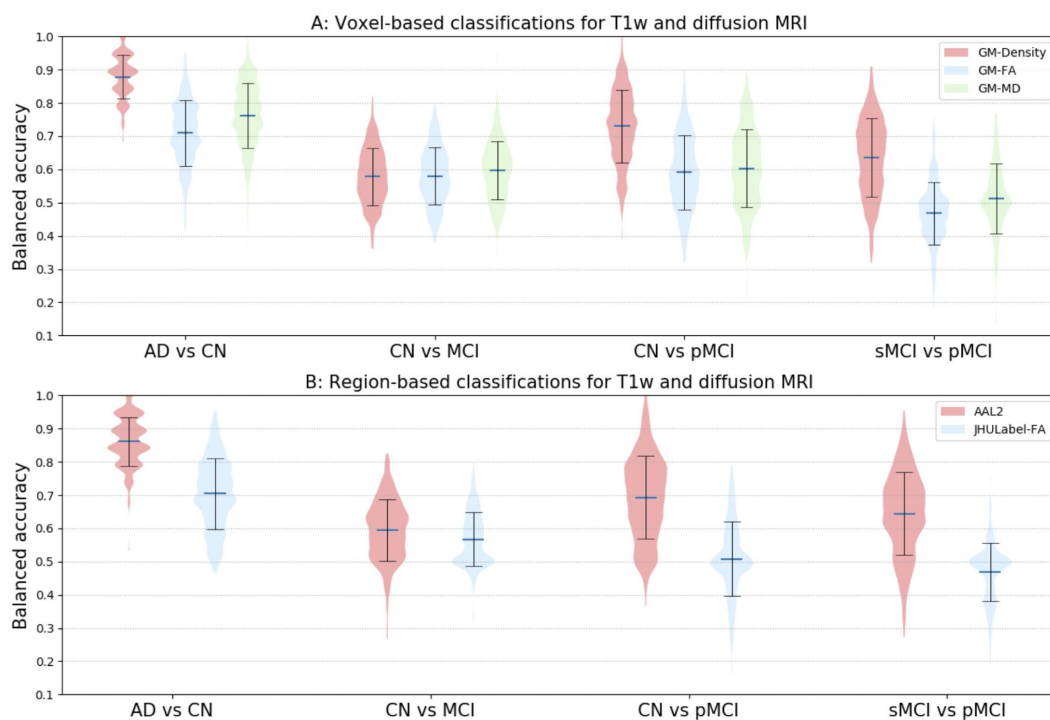


Figure 2. Distribution of the balanced accuracy obtained from both T1w and diffusion MRI for tasks CN vs AD, CN vs pMCI and sMCI vs pMCI. Both the results for voxel (top) and regional (bottom) feature with reference atlases are shown.

5.3 Influence of the imbalanced data

For voxel-wise classification, compared to the results of classification using imbalanced data, balanced data showed comparable accuracies for all three tasks, as shown in Figure 3. For MD region-wise approach, switching from imbalanced data to balanced data, accuracy considerably increased from 0.5 to 0.64 for task CN vs pMCI and from 0.5 to 0.59 for task CN vs MCI.

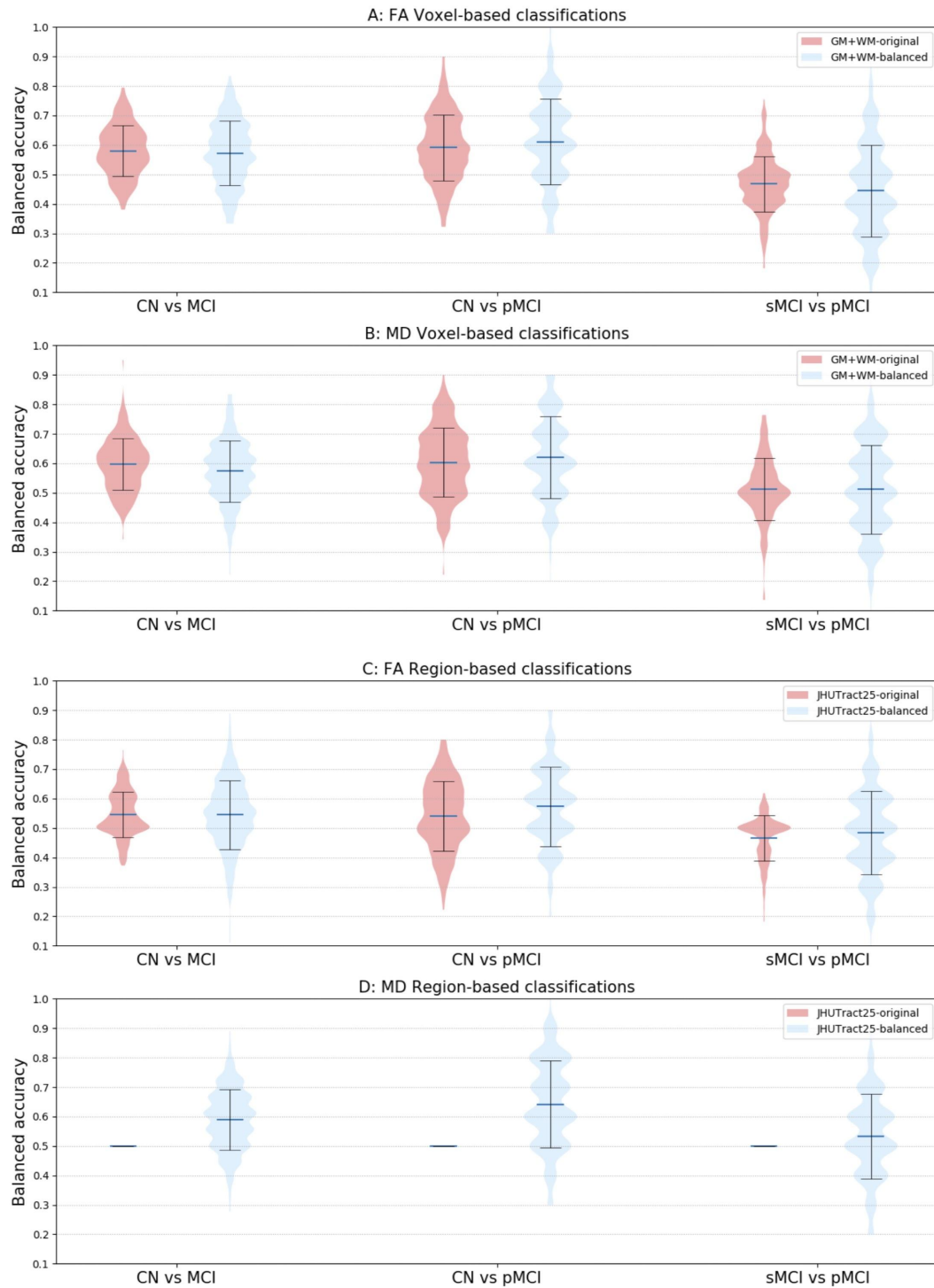


Figure 3. Distribution of the balanced accuracy obtained from the randomly balanced classifications for tasks CN vs MCI, CN vs pMCI and sMCI vs pMCI. For comparison, the original data classification results are also displayed. Both the results for voxel (top 2) and regional (bottom 2) feature are shown.

5.4 Influence of the feature selection bias

To assess the influence of FS bias, the experiments were restricted to GM+WM-FA and GM+WM-MD features for task CN vs AD, which are the cases with the highest number of features and for which the performance is higher. Results are presented in Figure 4.

For both FS algorithms, the non-nested approach resulted in vastly over-optimistic evaluations of performances, from 5% up to 40% increase in balanced accuracy. Specifically, for ANOVA, the highest balanced accuracy was obtained with the first 1% most informative voxels for non-nested approach (0.78 for FA and 0.83 for MD), and with all available voxels for nested approach (0.71 for FA and 0.76 for MD). For SVM-RFE, the highest balanced accuracy was achieved with the first 10% most informative voxels for non-nested approach (0.99 for FA and 0.83 for MD), and with the first 70% most informative voxels with FA (0.75) and the first 1% most informative voxels with MD (0.77) for nested approach. Compared to non-FS (no FS was performed), the nested ANOVA FS did not give better performance. Whilst while the nested SVM-RFE obtained slightly higher accuracies than non-FS: balanced accuracy increases from 0.71 (non-FS) to 0.75 (nested FS) for FA and 0.76 (non-FS) to 0.77 (nested FS) for MD.

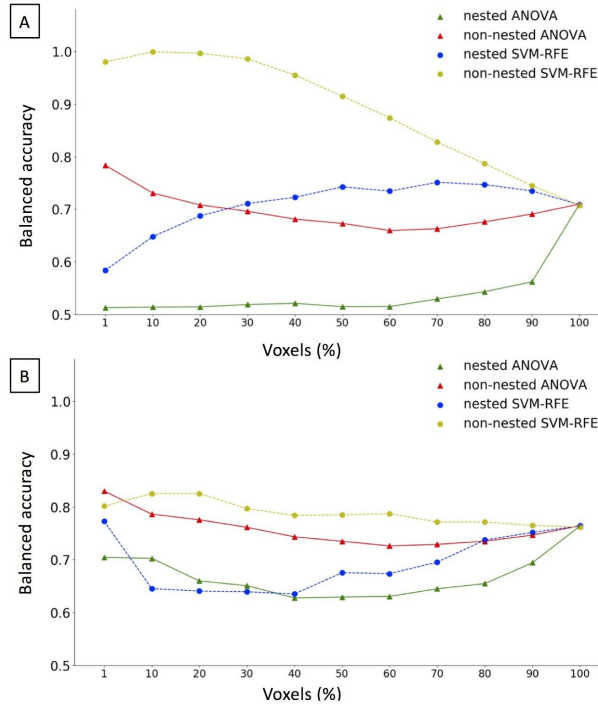


Figure 4. Balanced accuracy of CN vs AD obtained varying the number of voxels for ANOVA and SVM-RFE approaches. (A) GM+WM-FA feature; (B) GM+WM-MD feature.

5.5 Potential anatomical pattern

Figure 5 displays the OMH coefficient maps for the most successful task CN vs AD. For MD features, discriminative voxels were mainly within the GM (hippocampus and medial temporal cortex) (Figure 5B). When restricting the analysis to WM, only small regions were discriminative and these regions were outside those of the JHUTract25 atlas (Figure 5D), which is consistent with the poor performances obtained with MD regional features. For GM-density features (Figure 5C), the discriminative voxels also included these regions but were more extended (including some regions in the lateral temporal cortex and in the parietal and frontal lobes). For FA, discriminative voxels included both GM and WM regions (Figure 5A). In the GM, discriminative voxels were mainly located within the medial temporal lobe. In the WM, they were more diffuse and absent of the deep WM. These regions were close to the forceps minor and major tracts and inferior fronto-occipital fasciculus.

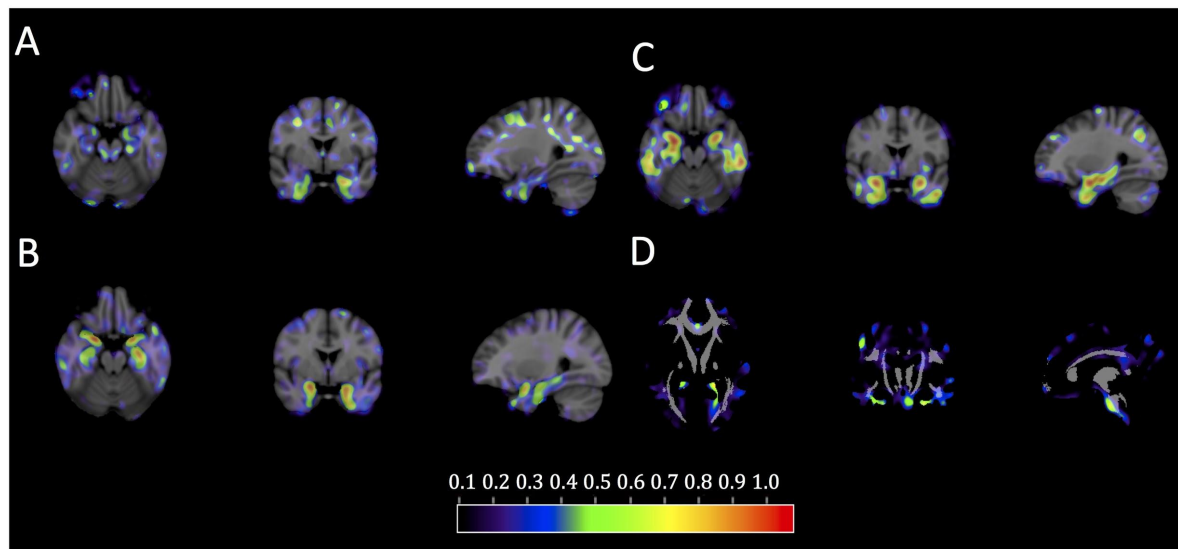


Figure 5. Normalized coefficient maps in MNI space. Task CN vs AD with A) GM+WM-FA features; B) GM+WM-MD features; C) GM-Density features; D) WM-MD features superimposed onto the JHUTract25 atlas (in gray). Warm colors, it means higher likelihood of classification into AD.

6. Discussion

In the present work, we proposed an open-source framework for the reproducible evaluation of AD classification from diffusion MRI, which extends our previous framework devoted to T1w MRI and PET. We demonstrated its use to assess the influence of different components on classification performances, specifically i) feature types, ii) imaging modalities (T1w MRI and diffusion MRI), iii) data imbalance and iv) FS strategies.

Generally, we hopefully contribute to make evaluation of machine learning approaches in AD more reproducible and more objective. Firstly, providing the tools to fully automatically convert original ADNI diffusion MRI into the community standard BIDS, we hope to facilitate the future work of researchers. Secondly, the literature (Uchida 2013; Cuingnet et al. 2011; Lu & Weng 2007) suggested that image processing procedures, including steps such as preprocessing, parcellation, registration and intensity normalization, have a strong influence on classification results. Hence, a standard diffusion MRI processing pipeline was proposed in the present work. Lastly, we proposed rigorous CV procedures following recent best practices (Varoquaux et al. 2017). The key components are publicly available in Clinica, a freely available software platform for clinical neuroscience research studies. We hope this framework will allow researchers to easily and rigorously evaluate their own classification algorithms, FS algorithms or image processing pipelines.

We then aimed to provide a baseline performance for future work. The results obtained in our framework were in line with the state-of-the-art. In our experiments, we obtained the balanced accuracy with 0.76 for task CN vs AD, 0.60 for task CN vs MCI and 0.61 for task CN vs pMCI. In general, the performances are low and support the idea that DTI metrics, alone, are not highly discriminant for AD classification. However, one can note that, in the literature, several studies using DTI-based features reported superior performances over our work (O'Dwyer et al. 2012; Nir et al. 2015; Demirhan et al. 2015; Mesrob et al. 2012; Termenon et

al. 2011; Graña et al. 2011). However, these discrepancies may come from i) the differences in image quality due to different dataset, ii) different sample size and iii) the FS bias, which we will specifically discuss below.

Different types of DTI-based features were assessed. Generally, voxel-wise features provided higher accuracies than region-wise features. This was consistent with a previous study (Demirhan et al. 2015), which reported accuracies of 0.75 for region-wise classification and of 0.88 for voxel-wise classification. Of note, the most discriminative voxels for WM-MD classification are outside the regions of the JHUTract25 atlas. This finding explains the poor performances obtained using MD regional features. Thus, the atlas used for region-wise approaches should be chosen with care. Moreover, FA and MD gave comparable performances for voxel-wise classification. This finding was supported by previous studies (Dyrba et al. 2013; Maggipinto et al. 2017; Lella et al. 2017). One study, which adopted a non-nested FS, reported that MD (accuracy of 0.81) outperformed FA (accuracy of 0.75) to discriminate CN from AD (Nir et al. 2015).

We also systematically compared the classification performance between T1w and diffusion MRI. The results showed that T1w MRI outperformed diffusion MRI. Several previous studies have compared the performances of these two modalities. Mesrob et al found that T1w MRI outperformed diffusion MRI (accuracy of 0.77 for T1w MRI vs 0.69 for FA from DTI) for task CN vs AD (Mesrob et al. 2012). However, their results were biased due to the adoption of a non-nested FS. Cui et al founded superior performance of T1w MRI over diffusion MRI (accuracy of 0.61 for T1w MRI vs 0.54 for FA from DTI) when classifying CN from MCI for both modalities (Cui et al. 2012). Using a predefined hippocampus ROI approach, Ahmed et al obtained comparable accuracies for both modalities for tasks CN vs AD (accuracy of 0.71 for T1w MRI vs 0.72 for MD from DTI) and CN vs MCI (accuracy of 0.65 for T1w MRI vs 0.68 for MD from DTI) (Ahmed et al. 2017). Given the larger sample size and

proper FS procedure in our work, we believe that the superior performances of T1w MRI over diffusion MRI is reliable and robust. Several factors could explain the better performances of T1w MRI. First, it is controversial but possible that WM degeneration is a secondary degenerative process compared to brain atrophy (Xie et al. 2006; Agosta et al. 2011). Another possibility is that ADNI diffusion MRI acquisitions used within our study do not make use of the state-of-the-art methods that impact on image quality. In particular, no fieldmap data is acquired which leads to suboptimal correction of magnetic susceptibility artifacts (Wu et al. 2008).

We evaluated the impact of data imbalance on the classification performance. It is commonly agreed that imbalanced data may adversely impact the classification performance as the learned model will be biased towards the majority class to minimize the overall error rate (Estabrooks 2000; Japkowicz & Others 2000; Dubey et al. 2014). Efforts have been made to deal with imbalanced data, which could be generally classified as algorithmic level (Akbani et al. 2004) and data level (Dubey et al. 2014). In the current study, for voxel-wise classification, we found that the low accuracies obtained in discriminating pMCI from sMCI or CN are potentially caused by the small sample size, rather than by the imbalanced data. Interestingly, Dubey et al showed that a balanced data obtained by several data resampling techniques gave better results than the imbalanced data using T1w MRI from ADNI (Dubey et al. 2014). Thus our hypothesis for the limited sample size needs to be further confirmed as more subjects are becoming available.

In the literature, researchers have emphasized that “double-dipping”, referring to the use of test subjects in any part of the training process, such as non-nested FS in this context, is bad practice and may lead to over-fitted classification (Kriegeskorte et al. 2009; Rathore et al. 2017b). Similarly, in a recent study, Maggipinto et al showed that the adoption of FS strategies should be taken with care (Maggipinto et al. 2017). They proved that a biased FS, usually a

non-nested FS, leads to over-optimistic results. Unfortunately, many previous studies using diffusion MRI for AD classification adopted the non-nested FS and reported nearly perfect classification (O'Dwyer et al. 2012; Mesrob et al. 2012; Graña et al. 2011). In the current study, our finding reinforced the message that non-nested FS could result in over-optimistic results. With the adoption of the non-nested SVM-RFE FS, a nearly perfect performance was achieved. Besides, FA outperformed MD for classification accuracies for this non-nested FS approach. Similar patterns were also witnessed in the study of Maggipinto et al (Maggipinto et al. 2017). Replacing the non-nested FS with the nested one, we obtained considerably inferior performances. On the other hand, we found that, with SVM-RFE not with ANOVA, the nested FS could potentially (slightly) improve the performance compared to the case no FS was performed. The difference between ANOVA and SVM-RFE may stem from the fact that ANOVA is performed for each feature (voxel) independently while GM and WM in contiguous voxels are highly correlated (Mechelli et al. 2005). Interestingly, another study found that, with the adoption of ReliefF algorithm, FS improved the classification accuracy up to 8% compared to the non-FS for task CN vs AD (Demirhan et al. 2015). However, they did not give enough details concerning their validation scheme. In particular, it is not clear if they used a nested FS (Demirhan et al. 2015).

Visualization of optimal margin hyperplane coefficient maps allowed to study which voxels contribute the most to the discrimination. FA, MD and GM-Density features shared a typical AD anatomical pattern: voxels in hippocampus and temporal lobe showed more discriminative ability in the classification. These findings were consistent with the literature. DTI-based group comparison analyses demonstrated altered FA or MD in the hippocampus (Fellgiebel et al. 2006; Kantarci et al. 2001; Müller et al. 2005; Müller et al. 2007; Hanyu et al. 1998) and in the temporal lobe (Hanyu et al. 1998; Fellgiebel et al. 2005; Head et al. 2005; Stahl et al. 2007). Moreover, the OMH coefficient map displayed a diffuse pattern for WM

voxels in our work. Similar patterns of WM voxels were also witnessed in the FS procedure using diffusion MRI (Demirhan et al. 2015; Dyrba et al. 2013).

Our study has the following limitations. First, ADNI diffusion MRI data was not acquired using the state-of-the-art methods which leads to suboptimal image quality. Related works have proven the negative impact of low image quality on MRI analyses (Yendiki et al. 2014; Alexander-Bloch et al. 2016; Reuter et al. 2015). It is thus possible that diffusion MRI acquired using more recent protocols would provide higher classification accuracies. Second, our experiments were performed with a limited data sample size. The limitation came from the data currently available in ADNI. In a previous study (Samper-González et al. 2018), we have demonstrated that increased training set size led to increased classification performances. Thus, both limitations can result in inferior classification performances. Lastly, our study only explored DTI-based features. With a proper CV and FS, more sophisticated features, such as brain tractography- or network-based features, could also be studied.

7. Acknowledgments

The research leading to these results has received funding from the program “Investissements d’avenir” ANR-10-IAIHU-06 (Agence Nationale de la Recherche-10-IA Institut Hospitalo-Universitaire-6) ANR-11-IDEX-004 (Agence Nationale de la Recherche-11- Initiative d’Excellence-004, project LearnPETMR number SU-16-R-EMR-16), from the European Union H2020 program (project EuroPOND, grant number 666992, project HBP SGA1 grant number 720270), from the joint NSF/NIH/ANR program “Collaborative Research in Computational Neuroscience” (project HIPLAY7, grant number ANR-16-NEUC-0001-01), from Agence Nationale de la Recherche (project PREVDEMALS, grant number ANR-14-CE15-0016-07), from the European Research Council (to Dr Durrleman project LEASP, grant number 678304), and from the Abeona Foundation (project Brain@Scale). J.W. receives financial support from China Scholarship Council (CSC). O.C. is supported by a “Contrat d’Interface Local” from Assistance Publique-Hôpitaux de Paris (AP-HP). N.B. receives funding from the People Programme (Marie Curie Actions) of the European Union’s Seventh Framework Programme (FP7/2007-2013) under REA grant agreement no. PCOFUND-GA-2013-609102, through the PRESTIGE programme coordinated by Campus France.

Data collection and sharing for this project was funded by the Alzheimer's Disease Neuroimaging Initiative (ADNI) (National Institutes of Health Grant U01 AG024904) and DOD ADNI (Department of Defense award number W81XWH-12-2-0012). ADNI is funded by the National Institute on Aging, the National Institute of Biomedical Imaging and Bioengineering, and through generous contributions from the following: AbbVie, Alzheimer’s Association; Alzheimer’s Drug Discovery Foundation; Araclon Biotech; BioClinica, Inc.; Biogen; Bristol-Myers Squibb Company; CereSpir, Inc.; Cogstate; Eisai Inc.; Elan Pharmaceuticals, Inc.; Eli Lilly and Company; EuroImmun; F. Hoffmann-La Roche Ltd and its affiliated company Genentech, Inc.; Fujirebio; GE Healthcare; IXICO Ltd.; Janssen

Alzheimer Immunotherapy Research & Development, LLC.; Johnson & Johnson Pharmaceutical Research & Development LLC.; Lumosity; Lundbeck; Merck & Co., Inc.; Meso Scale Diagnostics, LLC.; NeuroRx Research; Neurotrack Technologies; Novartis Pharmaceuticals Corporation; Pfizer Inc.; Piramal Imaging; Servier; Takeda Pharmaceutical Company; and Transition Therapeutics. The Canadian Institutes of Health Research is providing funds to support ADNI clinical sites in Canada. Private sector contributions are facilitated by the Foundation for the National Institutes of Health (www.fnih.org). The grantee organization is the Northern California Institute for Research and Education, and the study is coordinated by the Alzheimer's Therapeutic Research Institute at the University of Southern California. ADNI data are disseminated by the Laboratory for Neuro Imaging at the University of Southern California.

References

- Agosta, F., Pievani, M., Sala, S., Geroldi, C., Galluzzi, S., Frisoni, G. B., & Filippi, M. (2011). White matter damage in Alzheimer disease and its relationship to gray matter atrophy. *Radiology*, 258(3), 853–863. doi:10.1148/radiol.10101284
- Ahmed, O. B., Benois-Pineau, J., Allard, M., Catheline, G., & Amar, C. B. (2017). Recognition of Alzheimer's disease and Mild Cognitive Impairment with multimodal image-derived biomarkers and Multiple Kernel Learning. *Neurocomputing*, 220, 98–110. doi:10.1016/j.neucom.2016.08.041
- Akbani, R., Kwek, S., & Japkowicz, N. (2004). Applying Support Vector Machines to Imbalanced Datasets. In *Machine Learning: ECML 2004* (pp. 39–50). Springer Berlin Heidelberg. doi:10.1007/978-3-540-30115-8_7
- Alexander-Bloch, A., Clasen, L., Stockman, M., Ronan, L., Lalonde, F., Giedd, J., & Raznahan, A. (2016). Subtle in-scanner motion biases automated measurement of brain anatomy from in vivo MRI. *Human brain mapping*, 37(7), 2385–2397. doi:10.1002/hbm.23180
- Amoroso, N., Monaco, A., Tangaro, S., & Neuroimaging Initiative, A. D. (2017). Topological Measurements of DWI Tractography for Alzheimer's Disease Detection. *Computational and mathematical methods in medicine*, 2017, 5271627. doi:10.1155/2017/5271627
- Andersson, J. L. R., & Sotiropoulos, S. N. (2016). An integrated approach to correction for off-resonance effects and subject movement in diffusion MR imaging. *NeuroImage*, 125, 1063–1078. doi:10.1016/j.neuroimage.2015.10.019
- Ashburner, J. (2007). A fast diffeomorphic image registration algorithm. *NeuroImage*, 38(1), 95–113. doi:10.1016/j.neuroimage.2007.07.007
- Ashburner, J., & Friston, K. J. (2005). Unified segmentation. *NeuroImage*, 26(3), 839–851. doi:10.1016/j.neuroimage.2005.02.018

- Avants, B. B., Epstein, C. L., Grossman, M., & Gee, J. C. (2008). Symmetric diffeomorphic image registration with cross-correlation: evaluating automated labeling of elderly and neurodegenerative brain. *Medical image analysis*, 12(1), 26–41.
doi:10.1016/j.media.2007.06.004
- Bermingham, M. L., Pong-Wong, R., Spiliopoulou, A., Hayward, C., Rudan, I., Campbell, H., et al. (2015). Application of high-dimensional feature selection: evaluation for genomic prediction in man. *Scientific reports*, 5, 10312. doi:10.1038/srep10312
- Brookmeyer, R., Johnson, E., Ziegler-Graham, K., & Arrighi, H. M. (2007). Forecasting the global burden of Alzheimer's disease. *Alzheimer's & dementia: the journal of the Alzheimer's Association*, 3(3), 186–191. doi:10.1016/j.jalz.2007.04.381
- Cai, S., Huang, K., Kang, Y., Jiang, Y., von Deneen, K. M., & Huang, L. (2018). Potential biomarkers for distinguishing people with Alzheimer's disease from cognitively intact elderly based on the rich-club hierarchical structure of white matter networks. *Neuroscience research*. <https://www.sciencedirect.com/science/article/pii/S0168010218302232>
- Chandrashekar, G., & Sahin, F. (2014). A survey on feature selection methods. *Computers & Electrical Engineering*, 40(1), 16–28. doi:10.1016/j.compeleceng.2013.11.024
- Cuingnet, R., Gerardin, E., Tessieras, J., Auzias, G., Lehericy, S., Habert, M.-O., et al. (2011). Automatic classification of patients with Alzheimer's disease from structural MRI: a comparison of ten methods using the ADNI database. *NeuroImage*, 56(2), 766–781.
doi:10.1016/j.neuroimage.2010.06.013
- Cuingnet, R., Glaunès, J. A., Chupin, M., Benali, H., Colliot, O., & Alzheimer's Disease Neuroimaging Initiative. (2013). Spatial and Anatomical Regularization of SVM: A General Framework for Neuroimaging Data. *IEEE transactions on pattern analysis and machine intelligence*, 35(3), 682–696. doi:10.1109/TPAMI.2012.142

- Cui, Y., Wen, W., Lipnicki, D. M., Beg, M. F., Jin, J. S., Luo, S., et al. (2012). Automated detection of amnesic mild cognitive impairment in community-dwelling elderly adults: a combined spatial atrophy and white matter alteration approach. *NeuroImage*, 59(2), 1209–1217. doi:10.1016/j.neuroimage.2011.08.013
- Demirhan, A., Nir, T. M., Zavaliangos-Petropulu, A., Jack, C. R., Jr, Weiner, M. W., Bernstein, M. A., et al. (2015). FEATURE SELECTION IMPROVES THE ACCURACY OF CLASSIFYING ALZHEIMER DISEASE USING DIFFUSION TENSOR IMAGES. *Proceedings / IEEE International Symposium on Biomedical Imaging: from nano to macro. IEEE International Symposium on Biomedical Imaging*, 2015, 126–130. doi:10.1109/ISBI.2015.7163832
- Doan, N. T., Engvig, A., Persson, K., Alnæs, D., Kaufmann, T., Rokicki, J., et al. (2017). Dissociable diffusion MRI patterns of white matter microstructure and connectivity in Alzheimer's disease spectrum. *Scientific reports*, 7, 45131. doi:10.1038/srep45131
- Dubey, R., Zhou, J., Wang, Y., Thompson, P. M., Ye, J., & Alzheimer's Disease Neuroimaging Initiative. (2014). Analysis of sampling techniques for imbalanced data: An n = 648 ADNI study. *NeuroImage*, 87, 220–241. doi:10.1016/j.neuroimage.2013.10.005
- Dyrba, M., Barkhof, F., Fellgiebel, A., Filippi, M., Hausner, L., Hauenstein, K., et al. (2015). Predicting Prodromal Alzheimer's Disease in Subjects with Mild Cognitive Impairment Using Machine Learning Classification of Multimodal Multicenter Diffusion-Tensor and Magnetic Resonance Imaging Data. *Journal of neuroimaging: official journal of the American Society of Neuroimaging*, 25(5), 738–747. doi:10.1111/jon.12214
- Dyrba, M., Ewers, M., Wegrzyn, M., Kilimann, I., Plant, C., Oswald, A., et al. (2013). Robust automated detection of microstructural white matter degeneration in Alzheimer's disease using machine learning classification of multicenter DTI data. *PloS one*, 8(5), e64925. doi:10.1371/journal.pone.0064925

- Dyrba, M., Grothe, M., Kirste, T., & Teipel, S. J. (2015). Multimodal analysis of functional and structural disconnection in Alzheimer's disease using multiple kernel SVM. *Human brain mapping, 36*(6), 2118–2131. doi:10.1002/hbm.22759
- Ebadi, A., Dalboni da Rocha, J. L., Nagaraju, D. B., Tovar-Moll, F., Bramati, I., Coutinho, G., et al. (2017). Ensemble Classification of Alzheimer's Disease and Mild Cognitive Impairment Based on Complex Graph Measures from Diffusion Tensor Images. *Frontiers in neuroscience, 11*, 56. doi:10.3389/fnins.2017.00056
- Estabrooks, A. (2000). *A combination scheme for inductive learning from imbalanced data sets*. DalTech.
- Ewers, M., Sperling, R. A., Klunk, W. E., Weiner, M. W., & Hampel, H. (2011). Neuroimaging markers for the prediction and early diagnosis of Alzheimer's disease dementia. *Trends in neurosciences, 34*(8), 430–442. doi:10.1016/j.tins.2011.05.005
- Falahati, F., Westman, E., & Simmons, A. (2014). Multivariate data analysis and machine learning in Alzheimer's disease with a focus on structural magnetic resonance imaging. *Journal of Alzheimer's disease: JAD, 41*(3), 685–708. doi:10.3233/JAD-131928
- Fellgiebel, A., Dellani, P. R., Greverus, D., Scheurich, A., Stoeter, P., & Müller, M. J. (2006). Predicting conversion to dementia in mild cognitive impairment by volumetric and diffusivity measurements of the hippocampus. *Psychiatry research, 146*(3), 283–287. doi:10.1016/j.psychresns.2006.01.006
- Fellgiebel, A., Müller, M. J., Wille, P., Dellani, P. R., Scheurich, A., Schmidt, L. G., & Stoeter, P. (2005). Color-coded diffusion-tensor-imaging of posterior cingulate fiber tracts in mild cognitive impairment. *Neurobiology of aging, 26*(8), 1193–1198. doi:10.1016/j.neurobiolaging.2004.11.006
- Friese, U., Meindl, T., Herpertz, S. C., Reiser, M. F., Hampel, H., & Teipel, S. J. (2010). Diagnostic utility of novel MRI-based biomarkers for Alzheimer's disease: diffusion tensor

imaging and deformation-based morphometry. *Journal of Alzheimer's disease: JAD*, 20(2), 477–490. doi:10.3233/JAD-2010-1386

Frisoni, G. B., Fox, N. C., Jack, C. R., Jr, Scheltens, P., & Thompson, P. M. (2010). The clinical use of structural MRI in Alzheimer disease. *Nature reviews. Neurology*, 6(2), 67–77. doi:10.1038/nrneurol.2009.215

Gao, Y., Wee, C.-Y., Kim, M., Giannakopoulos, P., Montandon, M.-L., Haller, S., & Shen, D. (2015). MCI Identification by Joint Learning on Multiple MRI Data. *Medical image computing and computer-assisted intervention: MICCAI ... International Conference on Medical Image Computing and Computer-Assisted Intervention*, 9350, 78–85. doi:10.1007/978-3-319-24571-3_10

Gorgolewski, K., Burns, C. D., Madison, C., Clark, D., Halchenko, Y. O., Waskom, M. L., & Ghosh, S. S. (2011). Nipype: a flexible, lightweight and extensible neuroimaging data processing framework in python. *Frontiers in neuroinformatics*, 5, 13. doi:10.3389/fninf.2011.00013

Gorgolewski, K. J., Auer, T., Calhoun, V. D., Craddock, R. C., Das, S., Duff, E. P., et al. (2016). The brain imaging data structure, a format for organizing and describing outputs of neuroimaging experiments. *Scientific data*, 3, 160044. doi:10.1038/sdata.2016.44

Graña, M., Termenon, M., Savio, A., Gonzalez-Pinto, A., Echeveste, J., Pérez, J. M., & Besga, A. (2011). Computer aided diagnosis system for Alzheimer disease using brain diffusion tensor imaging features selected by Pearson's correlation. *Neuroscience letters*, 502(3), 225–229. doi:10.1016/j.neulet.2011.07.049

Guyon, I., Weston, J., Barnhill, S., & Vapnik, V. (2002). Gene Selection for Cancer Classification using Support Vector Machines. *Machine learning*, 46(1), 389–422. doi:10.1023/A:1012487302797

- Haller, S., Lovblad, K. O., & Giannakopoulos, P. (2011). Principles of classification analyses in mild cognitive impairment (MCI) and Alzheimer disease. *Journal of Alzheimer's disease: JAD*, 26 Suppl 3, 389–394. doi:10.3233/JAD-2011-0014
- Haller, S., Missonnier, P., Herrmann, F. R., Rodriguez, C., Deiber, M.-P., Nguyen, D., et al. (2013). Individual classification of mild cognitive impairment subtypes by support vector machine analysis of white matter DTI. *AJNR. American journal of neuroradiology*, 34(2), 283–291. doi:10.3174/ajnr.A3223
- Hanyu, H., Sakurai, H., Iwamoto, T., Takasaki, M., Shindo, H., & Abe, K. (1998). Diffusion-weighted MR imaging of the hippocampus and temporal white matter in Alzheimer's disease. *Journal of the neurological sciences*, 156(2), 195–200. doi:10.1016/S0022-510X(98)00043-4
- Head, D., Snyder, A. Z., Girton, L. E., Morris, J. C., & Buckner, R. L. (2005). Frontal-hippocampal double dissociation between normal aging and Alzheimer's disease. *Cerebral cortex*, 15(6), 732–739. doi:10.1093/cercor/bhh174
- Hua, K., Zhang, J., Wakana, S., Jiang, H., Li, X., Reich, D. S., et al. (2008). Tract probability maps in stereotaxic spaces: analyses of white matter anatomy and tract-specific quantification. *NeuroImage*, 39(1), 336–347. doi:10.1016/j.neuroimage.2007.07.053
- Japkowicz, N., & Others. (2000). Learning from imbalanced data sets: a comparison of various strategies. In *AAAI workshop on learning from imbalanced data sets* (Vol. 68, pp. 10–15). Menlo Park, CA. <http://www.aaai.org/Papers/Workshops/2000/WS-00-05/WS00-05-003.pdf>
- Jenkinson, M., Beckmann, C. F., Behrens, T. E. J., Woolrich, M. W., & Smith, S. M. (2012). FSL. *NeuroImage*, 62(2), 782–790. doi:10.1016/j.neuroimage.2011.09.015
- Jung, W. B., Lee, Y. M., Kim, Y. H., & Mun, C.-W. (2015). Automated Classification to Predict the Progression of Alzheimer's Disease Using Whole-Brain Volumetry and DTI. *Psychiatry investigation*, 12(1), 92–102. doi:10.4306/pi.2015.12.1.92

- Kantarci, K., Jack, C. R., Jr, Xu, Y. C., Campeau, N. G., O'Brien, P. C., Smith, G. E., et al. (2001). Mild cognitive impairment and Alzheimer disease: regional diffusivity of water. *Radiology*, 219(1), 101–107. doi:10.1148/radiology.219.1.r01ap14101
- Kriegeskorte, N., Simmons, W. K., Bellgowan, P. S. F., & Baker, C. I. (2009). Circular analysis in systems neuroscience: the dangers of double dipping. *Nature neuroscience*, 12(5), 535–540. doi:10.1038/nn.2303
- Leemans, A., & Jones, D. K. (2009). The B-matrix must be rotated when correcting for subject motion in DTI data. *Magnetic resonance in medicine: official journal of the Society of Magnetic Resonance in Medicine / Society of Magnetic Resonance in Medicine*, 61(6), 1336–1349. <http://onlinelibrary.wiley.com/doi/10.1002/mrm.21890/full>
- Lee, W., Park, B., & Han, K. (2013). Classification of diffusion tensor images for the early detection of Alzheimer's disease. *Computers in biology and medicine*, 43(10), 1313–1320. doi:10.1016/j.combiomed.2013.07.004
- Lee, W., Park, B., & Han, K. (2015). SVM-Based Classification of Diffusion Tensor Imaging Data for Diagnosing Alzheimer's Disease and Mild Cognitive Impairment. In D.-S. Huang, K.-H. Jo, & A. Hussain (Eds.), *Intelligent Computing Theories and Methodologies* (Vol. 9226, pp. 489–499). Cham: Springer International Publishing. doi:10.1007/978-3-319-22186-1_49
- Lella, E., Amoroso, N., Bellotti, R., Diacono, D., La Rocca, M., Maggipinto, T., et al. (2017). Machine learning for the assessment of Alzheimer's disease through DTI. In *Applications of Digital Image Processing XL* (Vol. 10396, p. 1039619). Presented at the Applications of Digital Image Processing XL, International Society for Optics and Photonics. doi:10.1117/12.2274140

- Lella, E., Amoroso, N., Lombardi, A., Maggipinto, T., Tangaro, S., Bellotti, R., & Estrada, E. (2018). Communicability disruption in Alzheimer's disease connectivity networks. *Journal of Complex Networks*. doi:10.1093/comnet/cny009
- Leow, A. D., Yanovsky, I., Chiang, M.-C., Lee, A. D., Klunder, A. D., Lu, A., et al. (2007). Statistical properties of Jacobian maps and the realization of unbiased large-deformation nonlinear image registration. *IEEE transactions on medical imaging*, 26(6), 822–832. doi:10.1109/TMI.2007.892646
- Li, M., Qin, Y., Gao, F., Zhu, W., & He, X. (2014). Discriminative analysis of multivariate features from structural MRI and diffusion tensor images. *Magnetic resonance imaging*, 32(8), 1043–1051. doi:10.1016/j.mri.2014.05.008
- Li, X., Morgan, P. S., Ashburner, J., Smith, J., & Rorden, C. (2016). The first step for neuroimaging data analysis: DICOM to NIfTI conversion. *Journal of neuroscience methods*, 264, 47–56. doi:10.1016/j.jneumeth.2016.03.001
- Lu, D., & Weng, Q. (2007). A survey of image classification methods and techniques for improving classification performance. *International journal of remote sensing*, 28(5), 823–870. doi:10.1080/01431160600746456
- Maggipinto, T., Bellotti, R., Amoroso, N., Diacono, D., Donvito, G., Lella, E., et al. (2017). DTI measurements for Alzheimer's classification. *Physics in medicine and biology*, 62(6), 2361–2375. doi:10.1088/1361-6560/aa5dbe
- Mechelli, A., Price, C. J., Friston, K. J., & Ashburner, J. (2005). Voxel-Based Morphometry of the Human Brain: Methods and Applications. *Current medical imaging reviews*, 1(2), 105–113. <https://www.ingentaconnect.com/content/ben/cmri/2005/00000001/00000002/art00001>
- Mesrob, L., Sarazin, M., Hahn-Barma, V., Souza, L. C. de, Dubois, B., Gallinari, P., & Kinkingnéhun, S. (2012). DTI and Structural MRI Classification in Alzheimer's Disease. *Advances in Molecular Imaging*, 02(02), 12–20. doi:10.4236/ami.2012.22003

- Müller, M. J., Greverus, D., Dellani, P. R., Weibrich, C., Wille, P. R., Scheurich, A., et al. (2005). Functional implications of hippocampal volume and diffusivity in mild cognitive impairment. *NeuroImage*, 28(4), 1033–1042. doi:10.1016/j.neuroimage.2005.06.029
- Müller, M. J., Greverus, D., Weibrich, C., Dellani, P. R., Scheurich, A., Stoeter, P., & Fellgiebel, A. (2007). Diagnostic utility of hippocampal size and mean diffusivity in amnesic MCI. *Neurobiology of aging*, 28(3), 398–403. doi:10.1016/j.neurobiolaging.2006.01.009
- Nir, T. M., Villalon-Reina, J. E., Prasad, G., Jahanshad, N., Joshi, S. H., Toga, A. W., et al. (2015). Diffusion weighted imaging-based maximum density path analysis and classification of Alzheimer's disease. *Neurobiology of aging*, 36 Suppl 1, S132–40. doi:10.1016/j.neurobiolaging.2014.05.037
- O'Dwyer, L., Lamberton, F., Bokde, A. L. W., Ewers, M., Faluyi, Y. O., Tanner, C., et al. (2012). Using support vector machines with multiple indices of diffusion for automated classification of mild cognitive impairment. *PloS one*, 7(2), e32441. doi:10.1371/journal.pone.0032441
- Petersen, R. C., Aisen, P. S., Beckett, L. A., Donohue, M. C., Gamst, A. C., Harvey, D. J., et al. (2010). Alzheimer's Disease Neuroimaging Initiative (ADNI): clinical characterization. *Neurology*, 74(3), 201–209. doi:10.1212/WNL.0b013e3181cb3e25
- Prasad, G., Joshi, S. H., Nir, T. M., Toga, A. W., Thompson, P. M., & Alzheimer's Disease Neuroimaging Initiative (ADNI). (2015). Brain connectivity and novel network measures for Alzheimer's disease classification. *Neurobiology of aging*, 36 Suppl 1, S121–31. doi:10.1016/j.neurobiolaging.2014.04.037
- Rathore, S., Habes, M., Iftikhar, M. A., Shacklett, A., & Davatzikos, C. (2017a). A review on neuroimaging-based classification studies and associated feature extraction methods for Alzheimer's disease and its prodromal stages. *NeuroImage*, 155, 530–548. doi:10.1016/j.neuroimage.2017.03.057

- Rathore, S., Habes, M., Iftikhar, M. A., Shacklett, A., & Davatzikos, C. (2017b). A review on neuroimaging-based classification studies and associated feature extraction methods for Alzheimer's disease and its prodromal stages. *NeuroImage*, *155*, 530–548.
doi:10.1016/j.neuroimage.2017.03.057
- Reuter, M., Tisdall, M. D., Qureshi, A., Buckner, R. L., van der Kouwe, A. J. W., & Fischl, B. (2015). Head motion during MRI acquisition reduces gray matter volume and thickness estimates. *NeuroImage*, *107*, 107–115. doi:10.1016/j.neuroimage.2014.12.006
- Rolls, E. T., Joliot, M., & Tzourio-Mazoyer, N. (2015). Implementation of a new parcellation of the orbitofrontal cortex in the automated anatomical labeling atlas. *NeuroImage*, *122*, 1–5.
doi:10.1016/j.neuroimage.2015.07.075
- Routier, A., Guillon, J., & Burgos, N. (2018). Clinica: an open source software platform for reproducible clinical neuroscience studies. *Annual meeting of the*. <https://hal.inria.fr/hal-01760658/>
- Samper-González, J., Burgos, N., Bottani, S., Fontanella, S., Lu, P., Marcoux, A., et al. (2018). Reproducible evaluation of classification methods in Alzheimer's disease: Framework and application to MRI and PET data. *NeuroImage*. doi:10.1016/j.neuroimage.2018.08.042
- Schouten, T. M., Koini, M., de Vos, F., Seiler, S., van der Grond, J., Lechner, A., et al. (2016). Combining anatomical, diffusion, and resting state functional magnetic resonance imaging for individual classification of mild and moderate Alzheimer's disease. *NeuroImage. Clinical*, *11*, 46–51. doi:10.1016/j.nicl.2016.01.002
- Schouten, T. M., Koini, M., Vos, F. de, Seiler, S., Rooij, M. de, Lechner, A., et al. (2017). Individual classification of Alzheimer's disease with diffusion magnetic resonance imaging. *NeuroImage*, *152*, 476–481. doi:10.1016/j.neuroimage.2017.03.025
- Selnes, P., Aarsland, D., Bjørnerud, A., Gjerstad, L., Wallin, A., Hessen, E., et al. (2013). Diffusion tensor imaging surpasses cerebrospinal fluid as predictor of cognitive decline and

medial temporal lobe atrophy in subjective cognitive impairment and mild cognitive impairment. *Journal of Alzheimer's disease: JAD*, 33(3), 723–736. doi:10.3233/JAD-2012-121603

Stahl, R., Dietrich, O., Teipel, S. J., Hampel, H., & Reiser, M. F. (2007). White Matter Damage in Alzheimer Disease and Mild Cognitive Impairment: Assessment with Diffusion-Tensor MR Imaging and Parallel Imaging Techniques¹. *Radiology*.

<http://pubs.rsna.org/doi/abs/10.1148/radiol.2432051714>

Termenon, M., Besga, A., Echeveste, J., Gonzalez-Pinto, A., & Graña, M. (2011). Alzheimer Disease Classification on Diffusion Weighted Imaging Features. In *New Challenges on Bioinspired Applications* (pp. 120–127). Springer Berlin Heidelberg. doi:10.1007/978-3-642-21326-7_14

Tournier, J.-D., Calamante, F., & Connelly, A. (2012). MRtrix: Diffusion tractography in crossing fiber regions. *International journal of imaging systems and technology*, 22(1), 53–66. doi:10.1002/ima.22005

Tustison, N. J., & Avants, B. B. (2013). Explicit B-spline regularization in diffeomorphic image registration. *Frontiers in neuroinformatics*, 7, 39. doi:10.3389/fninf.2013.00039

Uchida, S. (2013). Image processing and recognition for biological images. *Development, growth & differentiation*, 55(4), 523–549. doi:10.1111/dgd.12054

Varoquaux, G., Raamana, P. R., Engemann, D. A., Hoyos-Idrobo, A., Schwartz, Y., & Thirion, B. (2017). Assessing and tuning brain decoders: Cross-validation, caveats, and guidelines. *NeuroImage*, 145(Pt B), 166–179. doi:10.1016/j.neuroimage.2016.10.038

Vemuri, P., & Jack, C. R., Jr. (2010). Role of structural MRI in Alzheimer's disease. *Alzheimer's research & therapy*, 2(4), 23. doi:10.1186/alzrt47

Wang, Q., Guo, L., Thompson, P. M., Jack, C. R., Dodge, H., Zhan, L., et al. (2018). The Added Value of Diffusion-Weighted MRI-Derived Structural Connectome in Evaluating Mild

- Cognitive Impairment: A Multi-Cohort Validation¹. *Journal of Alzheimer's disease: JAD*, 64(1), 149–169. doi:10.3233/JAD-171048
- Wee, C.-Y., Yap, P.-T., Zhang, D., Denny, K., Browndyke, J. N., Potter, G. G., et al. (2012). Identification of MCI individuals using structural and functional connectivity networks. *NeuroImage*, 59(3), 2045–2056. doi:10.1016/j.neuroimage.2011.10.015
- Wu, M., Chang, L.-C., Walker, L., Lemaitre, H., Barnett, A. S., Marenco, S., & Pierpaoli, C. (2008). Comparison of EPI Distortion Correction Methods in Diffusion Tensor MRI Using a Novel Framework. In D. Metaxas, L. Axel, G. Fichtinger, & G. Székely (Eds.), *Medical Image Computing and Computer-Assisted Intervention – MICCAI 2008* (Vol. 5242, pp. 321–329). Berlin, Heidelberg: Springer Berlin Heidelberg. doi:10.1007/978-3-540-85990-1_39
- Xie, S., Xiao, J. X., Gong, G. L., Zang, Y. F., Wang, Y. H., Wu, H. K., & Jiang, X. X. (2006). Voxel-based detection of white matter abnormalities in mild Alzheimer disease. *Neurology*, 66(12), 1845–1849. doi:10.1212/01.wnl.0000219625.77625.aa
- Xie, Y., Cui, Z., Zhang, Z., Sun, Y., Sheng, C., Li, K., et al. (2015). Identification of Amnesic Mild Cognitive Impairment Using Multi-Modal Brain Features: A Combined Structural MRI and Diffusion Tensor Imaging Study. *Journal of Alzheimer's disease: JAD*, 47(2), 509–522. doi:10.3233/JAD-150184
- Yendiki, A., Koldewyn, K., Kakunoori, S., Kanwisher, N., & Fischl, B. (2014). Spurious group differences due to head motion in a diffusion MRI study. *NeuroImage*, 88, 79–90. doi:10.1016/j.neuroimage.2013.11.027
- Zhang, Y.-T., & Liu, S.-Q. (2018). Individual identification using multi-metric of DTI in Alzheimer's disease and mild cognitive impairment*. *Chinese Physics B*, 27(8), 088702. doi:10.1088/1674-1056/27/8/088702

- Zhan, L., Liu, Y., Wang, Y., Zhou, J., Jahanshad, N., Ye, J., et al. (2015). Boosting brain connectome classification accuracy in Alzheimer's disease using higher-order singular value decomposition. *Frontiers in neuroscience*, 9, 257. doi:10.3389/fnins.2015.00257
- Zhu, D., Li, K., Terry, D. P., Puente, A. N., Wang, L., Shen, D., et al. (2014). Connectome-scale assessments of structural and functional connectivity in MCI. *Human brain mapping*, 35(7), 2911–2923. doi:10.1002/hbm.22373